Structural, surface morphology, dielectric and magnetic properties of holmium doped BiFeO3 thin films prepared by pulsed laser deposition

Sadia Sharif, Ghulam Murtaza, Turgut Meydan, Paul I. Williams, Jerome Cuenca, Shaikh H. Hashimdeen, Fozia Shaheen, Riaz Ahmad

PII: S0040-6090(18)30494-2
DOI: doi:10.1016/j.tsf.2018.07.029
Reference: TSF 36786

To appear in: *Thin Solid Films*

Received date: 12 January 2018
Revised date: 19 July 2018
Accepted date: 20 July 2018

Please cite this article as: Sadia Sharif, Ghulam Murtaza, Turgut Meydan, Paul I. Williams, Jerome Cuenca, Shaikh H. Hashimdeen, Fozia Shaheen, Riaz Ahmad , Structural, surface morphology, dielectric and magnetic properties of holmium doped BiFeO3 thin films prepared by pulsed laser deposition. Tsf (2018), doi:10.1016/j.tsf.2018.07.029

Structural, surface morphology, dielectric and magnetic properties of holmium doped $BiFeO_3$ thin films prepared by pulsed laser deposition

Sadia Sharif[a], Ghulam Murtaza[b], Turgut Meydan[c], Paul I. Williams[c], Jerome Cuenca[c], Shaikh H. Hashimdeen[c], Fozia Shaheen[a], Riaz Ahmad[a]

[a]Department of Physics, GC University, Lahore-54000, Pakistan.
[b]Centre for Advanced Studies in Physics, GC University, Lahore-54000, Pakistan.
[c]Cardiff School of Engineering, Cardiff University, UK

Abstract

In this work, $Bi_{1-x}Ho_xFeO_3$ (with x = 0, 0.05, 0.10, 0.15 and 0.20) thin films were successfully grown on Si (100) substrates using pulsed laser deposition and the effect of Ho doping on the crystal structure, dielectric and magnetic properties were studied. X-ray diffraction studies on undoped $BiFeO_3$ confirmed the presence of a rhombohedral phase with crystallite sizes in the 14 - 24 nm range. The surface morphology and microstructure of the thin films were analysed by field emission scanning electron microscopy and atomic force microscopy. The results reveal that the grain size decreases as the Ho doping concentration increases. X-ray photoemission spectroscopy was used to identify the chemical bonding, valance band and core levels of Ho doped $BiFeO_3$ thin films. Dielectric constant and loss in Ho doped samples has been measured using a vector network analyzer and shows good dielectric behaviour compared to undoped $BiFeO_3$. A vibrating sample magnetometer was used to investigate the magnetic properties for Ho doping with concentrations of $x \geq 0.15$. In comparison to undoped $BiFeO_3$, the doped films exhibited larger remanence and saturation magnetization. The enhancement of these properties due to Ho doping is discussed along with their relevance in designing multiferroic materials based on $Bi_{1-x}Ho_xFeO_3$ films for magnetic field sensors, multiple-state memories and spintronic elements.

Key word: Bismuth ferrite, Thin Films, Pulsed laser deposition, Rare earth doping, Magnetism

1. Introduction

There has been growing interest in multiferroic materials owing to their exceptional properties and the simultaneous existence of both ferromagnetism and ferroelectricity (magneto-electric) in a single-phase distorted system. Due to these important properties, multiferroic materials have become an integral part of recent advances in magnetic media and information storage, multiple memory states, high-density ferroelectric random access memory, transducers, actuators, sensors, quantum electromagnets, spintronics and microelectronic devices [1–3]. Amongst the presently available multiferroic materials, $BiFeO_3$ (BFO) has attracted significant interest as it exhibits a magneto-electric coupling effect at room temperature in part due to a Néel temperature of 643 K (T_N) and a Curie temperature of 1103 K (T_C) [4–6]. This offers the prospect of controlling the electric polarization using magnetic fields or manipulating the magnetization through application of an electric field [7]. At room temperature, weak ferromagnetism can be introduced by chemically altering either the Fe-O-Fe bond angles or by changing the arrangements of the octahedral distribution of Fe^{2+} or Fe^{3+} ions [8]. In addition, the magnetic BFO structure exhibits G-type antiferromagnetism, in this type of structure each Fe^{3+} spin is surrounded by six antiparallel spins of the nearest Fe neighbours [9]. The exchange interaction is ferromagnetic along (100) planes in the neighbouring of Fe moments, while antiferromagnetic along [001] [9, 10]. The weak ferromagnetism is usually due to the canting of antiferromagnetic lattice when the orientation of magnetic moments of Fe^{3+} ions perpendicular to the [001] axis [11]. However, the weak ferromagnetism is not observed in practise because the antiferromagnetic spin structure in BFO is modified by a long-range cycloidal spiral modulated spin structure having spin periodicity of 62 nm [10] which cancels the macroscopic magnetization. The magnetization of BFO varies with applied electric field and/or stress, however, bismuth ferrites have some inherent drawbacks such as high leakage current, low dielectric constant and high tangent loss [12]. These problems have limited the applications of the material for electronic device applications [10]. Therefore, several attempts have been made in the last decade to solve these problems by doping with various ions at Bi/Fe-sites [13, 14]. $BiFeO_3$ is a rhombohedral distorted perovskite structure with a space group of R3c [15], where the A-sites are occupied by large ions belonging to the rare-earth, alkaline earth and alkali metals and the B-sites by transition metal cations. Thus, the

ferroelectric properties are due to the presence of 6s lone-pair electrons of B^{3+} ions and the ferromagnetism is due to the Fe^{3+} ions. It has already been reported that the substitution of lanthanides such as Sm and Tb [16], Nd^{+} [17], Eu^{+} [18], La+ [19], Ga^{+} [20] and Er [16, 21] on the Bi sites (A sites) produces a significant effect on the structural, magnetic and multiferroic performance of $BiFeO_3$ thin films [22]. The size of ionic radii of substituted ions also play an important role by inducing structural distortions which can lead to improve the multiferroic properties of $BiFeO_3$. Since, the difference in the ionic radii of Ho^{3+} (1.015 Å) and Bi^{3+} (1.20 Å) is significant , Bi sites in $BiFeO_3$ thin films have been substituted with Ho to induce structural distortion thereby reducing the concentration of oxygen vacancies (V_{ox}) and thus suppressing the volatility due to the presence of the Bi atoms [23].

Ho substitution may also suppress the spin structure, resulting in an increase in the canting angle of the anti-ferromagnetic coupled layers caused by tilting of the FeO_6 octahedra [24]. It has been noted that for Ho substitution in powdered and ceramic samples, the remanence and saturation magnetization can be enhanced, although nonmagnetic impurity phases may be present [25, 26]. Previous investigations have studied the influence of Ho doping on the multiferroic behaviour of $BiFeO_3$ thin films using various deposition techniques [16, 27–29] however, the pulsed laser deposition (PLD) technique is under-represented in this area. Therefore, in this work, $Bi_{1-x}FeO_3Ho_x$ thin films have been synthesized by using PLD and their multiferroic properties have been investigated.

2. Experimental detail

2.1. Chemicals used

The chemicals used to prepare the pure and doped $BiFeO_3$ films were Bismuth Oxide (Bi_2O_3) (Sigma-Aldrich purified 99.9 %), Ferric Oxide (Fe_2O_3) (Sigma-Aldrich purified 99.9 %) and Holmium Oxide (Ho_2O_3) (Sigma-Aldrich purified 99.9%). Poly Vinyl Alcohol (PVA) was also used in the synthesis process along with (100) silicon substrates.

2.2. Synthesis of Pure and doped bismuth ferrite

A conventional fabrication method was used to synthesize targets of pure and doped bismuth ferrite $Bi_{1-x}Ho_xFeO_3$ (with x = 0, 0.05, 0.10, 0.15 and 0.20) thin films. Stoichiometric proportions of powders Bi_2O_3, Fe_2O_3 and Ho_2O_3 (with excess of 2 mol % Bi_2O_3) were mixed thoroughly using an agate mortar and pestle for 2 hours. The well-grounded powder was calcined at 600 °C for 4 hours. The calcined powder was pressed into pellets of 2.54 cm

diameter and 3 - 4 mm thickness using PVA as a binder and a hydraulic pelletizer at an applied pressure of 98 kPa. Finally, the pellets were sintered at 850 °C for 2 hours.

2.3. Preparation of the thin films

$Bi_{1-x}Ho_xFeO_3$ thin films were deposited, using PLD, on to Si (100) substrates of size 10 × 10 cm that had been previously ultrasonically cleaned in distilled water and acetone followed by nitrogen flow drying. The PLD system was custom-built utilizing a Quantel France Nd:YAG 532 nm laser, model no. YG981C-10. Ablation of the $BiFeO_3$ target was achieved using 200 mJ laser pulses, with 6 ns duration at 10 Hz with a fluence of 1.5 J/cm^2. A full description of the system has previously been described [30]. Deposition parameters for the various thin films are listed in Table 1. The deposited films were finally sintered at 850 °C for 10 minutes in order to obtain a crystalline structure.

2.4. Characterizations

The orientation and phase composition of the thin films were determined using X-ray diffraction (XRD) (XPERT-PRO X-ray diffractometer) with a Cu-Kα source (λ = 1.5418 Å). XRD patterns were obtained with a 2θ range of 20° to 80° with step size 0.05°. Field emission scanning electron microscopy (FESEM, Zeiss NTS S360, Germany) was used to analyse the micro-structural cross-section of the thin films. The surface topography and other amplitude parameters of the $Bi_{1-x}Ho_xFeO_3$ thin films were evaluated by using Atomic Force Microscopy (AFM) (Model: 3100 Dimension, Veeco). Raman Spectra of the thin films were recorded using a Renishaw Raman spectrometer. X-ray photoelectron spectroscopy (XPS) (Make/ Model Kratoes Axis HSR, Japan) was used to investigate composition analysis and oxidation state of the multiferroic thin films. The room temperature frequency dependence of the complex dielectric properties were measured in the frequency range from 10 MHz to 10 GHz using a Vector Network Analyser (Agilent N5242A) and the open ended coaxial probe method. A detailed description of the set-up has been previously reported [31]. The magnetic hysteresis loops were measured by using a vibrating sample magnetometer (Model: 7400, Lake Shore).

3. Results and Discussion

3.1 Structure Analysis

XRD patterns of $Bi_{1-x}Ho_xFeO_3$ (x = 0, 0.05, 0.10, 0.15 and 0.20) thin films with different holmium concentrations are presented in Fig. 1. The peaks correspond well with the rhombohedral structure of pure $BiFeO_3$ (JCPDS file No. 00-014-0181) with a space group of R3c [32]. There is evidence of small amounts of $Bi_2Fe_4O_9$ and $Bi_{25}FeO_{40}$ phase formation in films with Ho concentrations of x = 0.05 and 0.20 respectively. Also, the main (110) peak slightly shifts toward higher values of 2θ with increasing Ho concentration. This is caused by the difference in the ionic radii of Ho^{3+} (1.015 Å) and Bi^{3+} (1.20 Å) stated previously, and as a consequence, the lattice constant decreases [16]. This observation also indicates that there is a distortion of rhombohedral structure as the presence of Ho ions at the Bi-sites results in a compression of the Fe-O bonds and a tension in the Bi-O bonds [33]. Scherer's equation is used to find out the average crystallite size of the thin films using X-ray line broadening [34].

$$D = 0.9\,\lambda/\,\beta\cos(\theta) \qquad (1)$$

Where, λ = 1.5405 Å, β is the full width at half maximum and θ is the Bragg angle. As the concentration of Ho increases, the calculated crystallite size of the thin films decreases as implied by the broadening of the peaks after doping as presented in table 2. A similar trend is reported in Dy-doped $BiFeO_3$ [35]. The Goldschmidt tolerance factor τ is used to determine the distortion and stability of the perovskite compound based on an ABO_3 formula [4]. Tolerance factor τ is calculated as follows:

$$\tau = \frac{1}{\sqrt{2}}\frac{\langle r_A\rangle + r_O}{\langle r_B\rangle + r_O} \qquad (2)$$

Where $\langle \mathbf{r_A} \rangle$ and $\langle \mathbf{r_B} \rangle$ are the average radii at A and B sites respectively, and r_o is the radius of O^{2-} ions. From equation 2, it has been seen that tolerance factor τ of $Bi_{1-x}Ho_xFeO_3$ thin films is reduced due to the average radius variation at A and B sites. This shows that increasing Ho content reduces the symmetry of the crystal structure.

3.2 SEM and AFM analysis

Fig. 2 shows the FESEM surface morphological features of the pure and Ho doped $BiFeO_3$ thin films. The cross-sectional view in Fig. 2(f), shows a uniformly deposited film with no inter diffusion with the silicon substrate and a thickness of around 174 nm. The microstructure of the thin film in Fig. 2(a) reveals that $BiFeO_3$ has a non-uniform

polycrystalline structure with distinct grain boundaries having an average size of 20±1 nm. Also, the porosity in the films decreases with Ho substitution. Since, the diffusivity of Ho^{3+} is less than Bi^{3+}, particle growth is reduced in the perovskite [35]. The reduction of the grain size with doping can be interpreted in terms of a reduction in V_{ox} [36]. The Bi-site substitution is more efficient to reduce oxygen vacancies in $BiFeO_3$ thin films [37]. The effect of Ho^{3+} doping on the surface morphology of the $BiFeO_3$ thin films has also been measured using AFM and confirms the presence of a granular microstructure, Fig. 3. The root mean square roughness varies from 40 to 60 nm and the grain size varies from 20 to 30 nm with Ho^{3+} substitution ranging from x = 0 to 0.15. Both FESEM and AFM observations show that Ho doping leads to the suppression of grain growth.

3.3. Raman Spectroscopy

A Raman spectra was obtained to analyse the structural development of Ho ion substituted $Bi_{1-x}Ho_xFeO_3$ thin films. The rhombohedral perovskite with a R3c space group under the frame work group theory analysis, has the Raman active mode which can be summarized using the following irreducible representation; $\Gamma = 4A_1 + 9E$ [38–40]. Fig. 4 depicts the Raman spectra of $BiHoFeO_3$ thin films having the wavenumber range 100 - 600 cm^{-1} at room temperature. Results reveal that all the Raman modes are well matched with the rhombohedrally distorted perovskite structure, which is in agreement with the literature [41]. In Fig. 4, the phonon modes at wavenumbers 138, 172.1, 226.6, 273.9, 345.9, 367.3 and 469.0 cm^{-1} were assigned as A_1-1, A_1-2, A_1-3, E3, E5, E6 and E7 respectively. A_1 modes (138, 172.1 cm^{-1}) are attributed to Bi–O covalent bonds [42]. In the present study, both the high intensity modes A_1-1 and A_1-2 shift to higher wavenumber values. This is because the average mass at Bi-sites decreases with partial substitution of Ho, which is approximately 21% lighter then Bi. The decrease in the intensity of A_1-1 and A_1-2 modes in the Ho ion substituted $BiFeO_3$ indicates a decline in the stereochemical activity of Bi^{3+} lone pair electrons which in turn changes the Bi–O bonds [43]. The change in the intensity of low value E modes indicates that Ho ion substitution at Bi sites affects the Bi-O bonds. Fig. 4 shows the variation in peak width and position for the A_1-1 phonon mode as a result of Bi-site substitution by Ho ions, a similar trend is also observed for the A_1-2 mode. This clearly shows that a decrease in the average Bi-site radius in $Bi_{1-x}Ho_xFeO_3$ thin films affects the Bi–O bonds and creates disorder in the lattice. For x = 0.20, all of the Raman modes have

disappeared, similar behaviour has also been observed in $Bi_{1-x}Nd_xFeO_3$ for x = 0.20 [43]. In the Raman spectrum of $Bi_{0.95}Ho_{0.05}FeO_3$, an additional mode at around 553 cm^{-1} was detected, this is attributed to a $Bi_2Fe_4O_9$ phase [44]. The appearance of this mode is in accordance with XRD data in which the presence of a secondary phase was also evident.

3.4 X-ray Photon Spectroscopy Analysis

To determine the charge transfer capability and chemical bonding in Ho doped $BiFeO_3$ thin films, the valance band and core levels of the elements were analysed using XPS. Fig. 5(a) shows the wide-range XPS survey spectra of $Bi_{1-x}Ho_xFeO_3$ thin films, peaks of different species such as Bi, Fe, O, and C elements have been identified. The C 1s peak at 285 eV is attributed to adventitious carbon and is used as a charge reference to rectify the binding energy of the XPS spectra [45]. Results in Fig. 5(a) reveal that there is no secondary holmium phase in metallic or oxide form. Therefore, Ho plays a vital role in occupying Bi sites, whilst maintaining the perovskite structure in accordance with XRD data [46]. Bi 4f and O 1s narrow scan spectra was fitted using the Gaussian-Lorentzian dividing peak analyses as shown in Fig. 5(b–c). The Bi 4f, Fe 2p, and O 1s peaks gradually shift towards higher binding energy regions, indicating an increase in bond strength between the atoms, which may be ascribed to Ho ions hybridizing with O ions to form stronger Ho-O bonds, and the interaction effect among the Bi-O, Fe-O and Ho-O bonds through the sharing of electron pairs [47]. Due to the spin orbit splitting, as shown in Fig. 5(b), the Bi ion consists of 4f7/2 and 4f5/2 core levels, which are located at 158.91/164.12, 158.34/164.20, 158.97/164.27, 158.99/ 164.30 and 159.22/ 164.35 eV for pure and doped $BiFeO_3$,. The sub-peaks located at the lower binding energy correspond to Bi vacancies and/or a relaxed Bi phase [48]. As Ho increases, the Bi-O bond energy progressively increases, leading to a more stable perovskite structure [49]. Fig. 5(c) depicts the plotted O1s narrow-scan spectra of pure and doped $BiFeO_3$, thin films. The spectra exhibits two distinct oxygen contributions (O_F and O_L) related to two sub-peaks located at 529.86/531.73, 529.63/531.47, 529.76/531.40, 529.69/531.91 and 529.59/531.49 eV for Ho concentrations of x = 0, 0.05, 0.1, 0.15 and 0.2 respectively. The former (O_F) can be attributed to the main peak of oxygen atoms in the samples lattice, while the latter (O_L) is related to the presence of oxygen vacancies [50]. The concentration ratios of O_F:O_L for Ho concentrations of x = 0, 0.05, 0.1, 0.15 and 0.2 are 71:29, 78:22, 74:24, 77:20 and 60:35 respectively, revealing that doping leads to a reduction in oxygen vacancies (V_{ox}).

Fig. 5(d) is the Fe 2p XPS spectra of the $BiFeO_3$ films showing Fe 2p1/2 and Fe 2p3/2 peaks. The binding energies calculated for the two types of iron ions (Fe^{2+} and Fe^{3+}) are 709.5 eV and 711 eV respectively [51]. The existence of Fe^{3+} is confirmed by the peak at 711.1 eV for the $Bi_{0.80}Ho_{0.20}FeO_3$ film and the existence of Fe^{2+} ions are indicated, at lower binding energies, by the presence of Fe 2p3/2 peaks for Ho substitutions with $x < 0.2$. The higher concentration of iron (Fe^{2+}) ions for low Ho compositions, confirms the prerequisite for charge compensation of oxygen vacancies [52].

3.5 Magnetic measurements

Fig. 6 presents the hysteresis loops of the $Bi_{1-x}Ho_xFeO_3$ films obtained at room temperature. It is clear that pure $BiFeO_3$ is less ferromagnetic compared to the Ho-doped specimens. The weak ferromagnetism in pure $BiFeO_3$ is due to the induced lattice distortion by heat treatment [53] and the effect of a spatially modulated spiral spin structure [54]. Results reveal that Ho substitution in $BiFeO_3$ enhances ferromagnetic ordering at room temperature. In Fig. 6, the coercive field measured 8.4, 8.3, 6.2, 7.0 and 5.2 kA/m for increasing composition of Ho together with an increase in saturation magnetization. The distortion in the lattice constant is a result of the difference in ionic radii of Ho^{3+} (1.015 Å) and Bi^{3+} (1.20 Å) ions. Therefore, in this work, no major structural phase changes occur for $x = 0.05$ and 0.1. The changes in inter atomic bond distances of Fe-O and Bi-O are associated with internal structural distortion and are also responsible for changes in magnetization. The bond angle and bond length are sensitive to super exchange interactions [55] and the structural distortion suppresses the spin spiral or alters the bond angle in Fe–O–Fe. It was observed that Ho^{3+} doping leads to an improvement in remanent magnetization (M_r). The appreciable variation in magnetization as a result of the Ho^{3+} doping is due to the well-known interactions: (T–T (Fe^{3+}–Fe^{3+}), R–T (Ho^{3+}–Fe^{3+}) and R–R (Ho^{3+}–Ho^{3+}) [56]. The substitution of Bi^{3+} with magnetically active Ho^{3+} ions causes the exchange interaction between the 4d sub-shell of Ho^{3+} and the 2p sub-shell of Fe^{3+}. This leads to an enhancement of the ferromagnetic properties of $Bi_{1-x}Ho_xFeO_3$, which is in good agreement with the literature [57].

3.6 Dielectric property

The dielectric constant (ε_r) and dielectric loss tangent ($\tan\delta$) for the pure and doped films are shown in Fig. 7(a, b) and Fig. 8(a, b) respectively. Results show that ε_r is almost frequency

independent in the MHz to the low GHz range. A decrease is noticed at frequencies approaching 10 GHz. It must be stipulated that the standard deviation errors are larger than any differences seen in the data for compositions x = 0.00 to 0.15 as shown in Fig. 7(a, b) and Fig. 8(a, b), hence, no discernible conclusions can be drawn from samples in this doping range. At a Ho concentration of x = 0.20 however, it is clear that the dielectric constant and loss tangent have decreased significantly.

In this frequency range, the dielectric properties are due to a combination of polarization mechanisms i.e. interfacial, ionic and atomic. Interfacial polarization occurs at the interface between two contrasting dielectric materials where the application of an electric field causes charges to bunch at the interface between the two materials, creating regions of space charge [34, 58]. Ionic polarization is associated with the flow of ions in a material (whether they are free in solution or, most likely in this case, the apparent conduction of lattice ions through double-exchange electron hopping). Finally, atomic polarization contributes through displacement of positive and negative charges in the atom itself. Structural defects in the material, including macroscopic porosity and microscopic structural defects are expected to play large roles in the polarization [59]. High porosity introduces interfaces and therefore high concentrations of space charge, resulting in a large dielectric constant (as is seen in the pure $BiFeO_3$ sample) [58]. The decrease in porosity with Ho doping may provide an explanation towards its decreasing ε_r and $\tan\delta$. Microscopic structural defects, however, may disrupt long range electron hopping paths through each grain. As the grain size reduces, so too does the conductivity and consequently, both dielectric loss and the leakage current decreases [60]. Hence, with this dielectric spectroscopy approach, we can indirectly infer that Ho substitution may decrease the leakage current of the $BiFeO_3$ thin films at x = 0.2, however direct measurement of leakage current is needed to confirm this hypothesis.

Conclusion

Ho doped $BiFeO_3$ multiferroic thin films were deposited using a PLD method. XRD analysis confirmed a variation in the lattice parameters with increasing holmium content and an impurity phase was observed for high Ho concentrations i.e. $x \geq 0.15$. FESEM and AFM micrographs show Ho reduces the particle size leading to the formation of island-like structures. XPS analysis shows that the concentration of Fe^{2+} reduces with increasing holmium content, leading to the suppression of oxygen vacancies. The saturation magnetization M_s increases while coercivity decreases with Ho doping and we summarize that enhancement of magnetization is due to the presence of magnetic Ho ions. The dielectric

properties are also affected by Ho content but only for compositions above x = 0.2 leading to a reduced dielectric constant. These results demonstrate that Ho, as a dopant, is effective in tuning the properties of multiferroic $BiFeO_3$ films and therefore offers the prospect for development of these materials for a range of future applications.

Acknowledgement

This work was supported by the Higher Education Commission Government of Pakistan under International Research support initiative Program (IRISP) awarded to Sadia Sharif. We are also thankful to Dr. Khaliq Mahmood for providing us the thin film deposition facility (PLD) at CASP, GC University, Lahore, Pakistan.

References

[1] S.-W. Cheong and M. Mostovoy, Multiferroics: a magnetic twist for ferroelectricity, Nat. Mater. 6 (2007) 13-20.
[2] R. Zeches, M. Rossell, J. Zhang, A. Hatt, Q. He, C.-H. Yang, A. Kumar, C. Wang, A. Melville and C. Adamo, A strain-driven morphotropic phase boundary in $BiFeO_3$, Science 326 (2009) 977-980.
[3] B. Yu, M. Li, J. Liu, D. Guo, L. Pei and X. Zhao, Effects of ion doping at different sites on electrical properties of multiferroic $BiFeO_3$ ceramics, J. Phys. D: Appl. Phys. 41 (2008) 065003.
[4] K. Chakrabarti, K. Das, B. Sarkar and S. De, Magnetic and dielectric properties of Eu-doped $BiFeO_3$ nanoparticles by acetic acid-assisted sol-gel method, J. Appl. Phys. 110 (2011) 103905.
[5] M. Li, M. Ning, Y. Ma, Q. Wu and C. Ong, Room temperature ferroelectric, ferromagnetic and magnetoelectric properties of Ba-doped $BiFeO_3$ thin films, J. Phys. D: Appl. Phys. 40 (2007) 1603-1607.
[6] R. Thomas, J. Scott, D. N. Bose and R. S. Katiyar, Multiferroic thin-film integration onto semiconductor devices, J. Phys. Condens. Matter 22 (2010) 423201.
[7] W. Xing, Y. Ma, Z. Ma, Y. Bai, J. Chen and S. Zhao, Improved ferroelectric and leakage current properties of Er-doped $BiFeO_3$ thin films derived from structural transformation, Smart Mater. Struct. 23 (2014) 085030.
[8] W. Prellier, M. Singh and P. Murugavel, The single-phase multiferroic oxides: from bulk to thin film, J. Phys.: Condens. Matter 17 (2005) R803.
[9] I. Sosnowska, T. P. Neumaier and E. Steichele, Spiral magnetic ordering in bismuth ferrite, J. Phys. C: Solid State Phys. 15 (1982) 4835-4846.
[10] D. Lebeugle, D. Colson, A. Forget, M. Viret, P. Bonville, J.-F. Marucco and S. Fusil, Room-temperature coexistence of large electric polarization and magnetic order in $BiFeO_3$ single crystals, Phys. Rev. B 76 (2007) 024116.
[11] C. Ederer and N. A. Spaldin, Weak ferromagnetism and magnetoelectric coupling in bismuth ferrite, Phys. Rev. B 71 (2005) 060401.
[12] Y. Wang, L. Zhou, M. Zhang, X. Chen, J.-M. Liu and Z. Liu, Room-temperature saturated ferroelectric polarization in $BiFeO_3$ ceramics synthesized by rapid liquid phase sintering, Appl. Phys. Lett. 84 (2004) 1731-1733.
[13] G. Yuan, S. W. Or, J. Liu and Z. Liu, Structural transformation and ferroelectromagnetic behavior in single-phase $Bi_{1-x}Nd_xFeO_3$ multiferroic ceramics, Appl. Phys. Lett. 89 (2006) 052905.
[14] J.-B. Li, G. Rao, J. Liang, Y. Liu, J. Luo and J. Chen, Magnetic properties of $Bi(Fe_{1-x}Cr_x)O_3$ synthesized by a combustion method, Appl. Phys. Lett. 90 (2007) 162513.
[15] A. A. Saad, W. Khan, P. Dhiman, A. Naqvi and M. Singh, Structural, optical and magnetic properties of perovskite $(La_{1-x}Sr_x)(Fe_{1-x}Ni_x)O_3$, (x = 0.0, 0.1 & 0.2) nanoparticles, Electron. Mater. Lett. 9 (2013) 77-81.
[16] Y. Liu, Y. Wang, J. Zhang, M. Gao, Y. Zhang, M. Wei and J. Yang, Effect of Ho substitution on structure and magnetic property of $BiFeO_3$ prepared by sol–gel method, Mater. Sci. Semicond. Process. 40 (2015) 787-795.
[17] H. Uchida, R. Ueno, H. Funakubo and S. Koda, Crystal structure and ferroelectric properties of rare-earth substituted $BiFeO_3$ thin films, J. Appl. Phys. 100 (2006) 014106.
[18] A. Lahmar, S. Habouti, M. Dietze, C. Solterbeck and M. Es-Souni, Effects of rare earth manganites on structural, ferroelectric, and magnetic properties of $BiFeO_3$ thin films, Appl. Phys. Lett. 94 (2009) 12903.
[19] A. Z. Simões, M. Ramirez, C. Foschini, F. Moura, J. A. Varela and E. Longo, Enhanced ferroelectric properties of La-substituted $BiFeO_3$ thin films on $LaSrCoO_3/Pt/TiO_2/SiO_2/Si$ (100) substrates prepared by the soft chemical method, Ceram. Int. 38 (2012) 3841-3849.
[20] V. Khomchenko, V. Shvartsman, P. Borisov, W. Kleemann, D. Kiselev, I. Bdikin, J. Vieira and A. Kholkin, Crystal structure and magnetic properties of $Bi_{0.8}(Gd_{1-x}Ba_x)_{0.2}FeO_3$ (x = 0, 0.5, 1) multiferroics J. Phys. D: Appl. Phys. 42 (2009) 045418.

[21] Y. Liu, J. Zhang, Y. Wu, Y. Zhang, M. Wei and J. Yang, Enhancement of magnetization in Er doped $BiFeO_3$ thin Film, J. Sol-Del Sci. Technol. 67 (2013) 1-7.
[22] W. Ye, G. Tan, G. Dong, H. Ren and A. Xia, Improved multiferroic properties in (Ho, Mn) co-doped $BiFeO_3$ thin films prepared by chemical solution deposition, Ceram. Int. 41 (2015) 4668-4674.
[23] H. Uchida, R. Ueno, H. Nakaki, H. Funakubo and S. Koda, Ion modification for improvement of insulating and ferroelectric properties of $BiFeO_3$ thin films fabricated by chemical solution deposition, Jpn. J. Appl. Phys. 44 (2005) L561.
[24] S. Singh, H. Ishiwara and K. Maruyama, Room temperature ferroelectric properties of Mn-substituted $BiFeO_3$ thin films deposited on Pt electrodes using chemical solution deposition, Appl. Phys. Lett. 88 (2006) 262908-262908.
[25] S. Pradhan, J. Das, P. Rout, V. Mohanta, S. Das, S. Samantray, D. Sahu, J. Huang, S. Verma and B. Roul, Effect of holmium substitution for the improvement of multiferroic properties of $BiFeO_3$, J Phys. Chem. Solids 71 (2010) 1557-1564.
[26] Z.-L. Hou, H.-F. Zhou, L.-B. Kong, H.-B. Jin, X. Qi and M.-S. Cao, Enhanced ferromagnetism and microwave absorption properties of $BiFeO_3$ nanocrystals with Ho substitution, Mater. Lett. 84 (2012) 110-113.
[27] W. Ye, G. Tan, G. Dong, H. Ren and A. Xia, Improved multiferroic properties in (Ho, Mn) co-doped BiFeO 3 thin films prepared by chemical solution deposition, Ceram. Int. 41 (2015) 4668-4674.
[28] Y. Qi, B. Alima and Z. Shifeng, Lattice distortion of holmium doped bismuth ferrite nanofilms, J. Rare Earths 32 (2014) 884-889.
[29] C. Park, Y. Shon, I. Yoon and J. Son, Multiferroic characteristics of the strained epitaxial $Bi_{0.9}Ho_{0.1}FeO_3$ thin film, Curr. Appl. Phys. 13 (2013) 386-389.
[30] K. Mahmood, S. Bashir, M. Khaleeq-Ur-Rahman, N. Farid, M. Akram, A. Hayat and Faizan-Ul-Haq, Effects of substrate temperature on structural, optical and surface morphological properties of pulsed laser deposited ZnO thin films, Surf. Rev. Lett. 20 (2013) 1350032.
[31] J. A. Cuenca, E. Thomas, S. Mandal, O. Williams and A. Porch, Investigating the broadband microwave absorption of nanodiamond impurities, IEEE Trans. Microw. Theory Tech. 63 (2015) 4110-4118.
[32] I. Sosnowska, R. Przeniosło, P. Fischer and V. Murashov, Neutron diffraction studies of the crystal and magnetic structures of $BiFeO_3$ and $Bi_{0.93}La_{0.07}FeO_3$, J. Magn. Magn. Mater. 160 (1996) 384-385.
[33] T. Durga Rao, R. Ranjith and S. Asthana, Enhanced magnetization and improved insulating character in Eu substituted $BiFeO_3$, J. Appl. Phys. 115 (2014) 124110.
[34] S. Pattanayak, R. Choudhary, P. R. Das and S. Shannigrahi, Effect of Dy-substitution on structural, electrical and magnetic properties of multiferroic $BiFeO_3$ ceramics, Ceram. Int. 40 (2014) 7983-7991.
[35] Y. Ma, W. Xing, J. Chen, Y. Bai, S. Zhao and H. Zhang, The influence of Er, Ti co-doping on the multiferroic properties of $BiFeO_3$ thin films, Appl. Phys. A 122:63 (2016).
[36] Q. Yun, W. Xing, J. Chen, W. Gao, Y. Bai and S. Zhao, Effect of Ho and Mn co-doping on structural, ferroelectric and ferromagnetic properties of $BiFeO_3$ thin films, Thin Solid Films 584 (2015) 103-107.
[37] N. Panwar, I. Coondoo, A. Tomar, A. Kholkin, V. S. Puli and R. S. Katiyar, Nanoscale piezoresponse and magnetic studies of multiferroic Co and Pr co-substituted BFO thin films, Mater. Res. Bull. 47 (2012) 4240-4245.
[38] M. K. Singh, H. M. Jang, S. Ryu and M.-H. Jo, Polarized Raman scattering of multiferroic $BiFeO_3$ epitaxial films with rhombohedral R3c symmetry, Appl. Phys. Lett. 88 (2006) 042907.
[39] R. Haumont, J. Kreisel, P. Bouvier and F. Hippert, Phonon anomalies and the ferroelectric phase transition in multiferroic $BiFeO_3$, Phys. Rev. B, 73 (2006) 132101.
[40] H. Fukumura, H. Harima, K. Kisoda, M. Tamada, Y. Noguchi and M. Miyayama, Raman scattering study of multiferroic $BiFeO_3$ single crystal, J. Magn. Magn. Mater. 310 (2007) e367-e369.
[41] P. Hermet, M. Goffinet, J. Kreisel and P. Ghosez, Raman and infrared spectra of multiferroic bismuth ferrite from first principles, Phys. Rev. B, 75 (2007) 220102.

[42] J. Lin, T. Tite, Y. Tang, C. Lue, Y. Chang and J. Lin, Correlation of spin and structure in doped bismuth ferrite nanoparticles, J. Appl. Phys. 111 (2012) 07D910.
[43] G. Yuan, S. W. Or and H. L. W. Chan, Raman scattering spectra and ferroelectric properties of $Bi_{1-x}Nd_xFeO_3$ (x = 0 - 0.2) multiferroic ceramics, J. Appl. Phys. 101 (2007) 064101.
[44] M. Iliev, A. Litvinchuk, V. Hadjiev, M. Gospodinov, V. Skumryev and E. Ressouche, Phonon and magnon scattering of antiferromagnetic $Bi_2Fe_4O_9$, Phys. Rev. B, 81 (2010) 024302.
[45] P. W. Wang, M. Guttag and C.-S. Tu, Surface Modification of Multiferroic $BiFeO_3$ Ceramic by Argon Sputtering, J. Surf. Eng. Mater. Adv. Technol. 4 (2014) 295-308.
[46] X. Xue, G. Tan, H. Hao and H. Ren, Comparative study on substitution effects in $BiFeO_3$ thin films fabricated on FTO substrates by chemical solution deposition, Appl. Surf. Sci. 282 (2013) 432-438.
[47] X. Xue, G. Tan, W. Liu and H. Ren,Nd doping effect on $Bi_{1-x}Nd_xFe_{0.97}Co_{0.03}O_3$ thin films: microstructural, electrical, optical and enhanced multiferroic properties, Mater. Chem. Phys. 146 (2014) 183-191.
[48] Z. Quan, W. Liu, H. Hu, S. Xu, B. Sebo, G. Fang, M. Li and X. Zhao, Microstructure, electrical and magnetic properties of Ce-doped $BiFeO_3$ thin films, J. Appl. Phys. 104 (2008) 084106.
[49] X. Xue, G. Tan, H. Hao and H. Ren, Comparative study on substitution effects in $BiFeO_3$ thin films fabricated on FTO substrates by chemical solution deposition, Appl. Surf. Sci. 282 (2013) 432-438.
[50] S. Wang, W. Liu, J. Gao, X. Qiu, Y. Feng, X. Hou, D. Yu and D. Li, Resistive switching and threshold switching behaviors in $La_{0.1}Bi_{0.9}Fe_{1-x}Co_xO_3$ ceramics, J. Appl. Phys. 112 (2012) 034110.
[51] J. Wei and D. Xue,Effect of non-magnetic doping on leakage and magnetic properties of $BiFeO_3$ thin films, Appl. Surf. Sci. 258 (2011) 1373-1376.
[52] Y. Shuai, S. Zhou, D. Bürger, M. Helm and H. Schmidt, Nonvolatile bipolar resistive switching in Au/$BiFeO_3$/Pt, J. Appl. Phys. 109 (2011), pp. 124117.
[53] X. Zheng, Q. Xu, Z. Wen, X. Lang, D. Wu, T. Qiu and M. Xu, The magnetic properties of La doped and codoped $BiFeO_3$, J. Alloys Compd. 499 (2010) 108-112.
[54] W. Liu, G. Tan, X. Xue, G. Dong, H. Ren and A. Xia, Phase transition and enhanced multiferroic properties of (Sm, Mn and Cr) co-doped $BiFeO_3$ thin films, Ceram. Int. 40 (2014) 12179-12185.
[55] A. Kumar, K. Yadav and J. Rani, Low temperature step magnetization and magnetodielectric study in $Bi_{0.95}La_{0.05}Fe_{1-x}Zr_xO_3$ ceramics, Mater. Chem. Phys. 134 (2012) 430-434.
[56] Y. Liu, Y. Wang, J. Zhang, M. Gao, Y. Zhang, M. Wei and J. Yang, Effect of Ho substitution on structure and magnetic property of $BiFeO_3$ prepared by sol–gel method, Mater. Sci. Semicond. Process. 40 (2015) 787-795.
[57] W. Xing, Y. Ma, J. Chen and S. Zhao, Enhanced Multiferroic Properties of Eu-Doped $BiFeO_3$ Thin Films Derived from Rhombohedral-Tetragonal Phase Boundary, J. Electron. Mater. 44 (2015) 3752-3760.
[58] B. Barick, K. Mishra, A. Arora, R. Choudhary and D. K. Pradhan,Impedance and Raman spectroscopic studies of $(Na_{0.5}Bi_{0.5})TiO_3$, J. Phys. D: Appl. Phys. 44 (2011) 355402.
[59] S. Pattanayak, R. Choudhary and P. R. Das, Effect of Gd-substitution on phase transition and conduction mechanism of $BiFeO_3$, J. Mater. Sci.: Mater. Electron. 24 (2013) 2767-2771.
[60] R. Mishra, D. K. Pradhan, R. Choudhary and A. Banerjee, Effect of yttrium on improvement of dielectric properties and magnetic switching behavior in $BiFeO_3$, J. Phys.: Condens. Matter 20 (2008) 045218.

Figures and Table Captions

Fig. 1. XRD spectra of Ho doped $BiFeO_3$ (with x = 0.0 to 0.20) thin films on Si (100) substrate sintered at 800 °C for 1 hour.

Fig. 2. FE-SEM micrographs for surface morphology of the Ho doped $BiFeO_3$ (with x = 0.0 to 0.20) thin films sintered at 800 °C for 1 hour.

Fig. 3. AFM images of $Bi_{1-x}Ho_xFeO_3$ thin films (a) x = 0, (b) x = 0.05, (c) x = 0.10 and (d) x = 0.15.

Fig. 4. Raman spectra of $Bi_{1-x}Ho_xFeO_3$ (x = 0 to 0.20) thin films at room temperature

Fig. 5. XPS spectra of $Bi_{1-x}Ho_xFeO_3$ (x = 0 to 0.20) thin films sintered at 800 °C for 1 hour showing (a) a wide-scan, and narrow-scans of (b) Bi 4f, (c) O 1s and (d) Fe 2p signals.

Fig. 6. Magnetic hysteresis loops of the $Bi_{1-x}Ho_xFeO_3$ (x = 0.0 to 0.20) films obtained at room temperature and sintered at 800 °C for 1 hour.

Fig. 7. Dielectric constant of Ho doped $Bi_{1-x}Ho_xFeO_3$ (x = 0.0 to 0.20) thin film (a) without and (b) with standard deviation.

Fig. 8. Dissipation factor (tanδ) of Ho doped $Bi_{1-x}Ho_xFeO_3$ (x = 0.0 to 0.20) thin film (a) without and (b) with standard deviation.

Table 1: Optimized deposition parameters for PLD

Laser type	Nd:YAG (532 nm)
Substrate temperature	400 ^{o}C
Target rotation speed	2 rpm
Laser density	1.5 J/cm^{2}
Target to substrate distance	4 cm
Base pressure	0.133 Pa
O_2 Pressure	33.3 Pa
Repetition rate	10 Hz
No. of pulses	6000
Time	10 minutes

Table 2: The structural parameters (a, c, V, D) and t (tolerance factor) for $Bi_{1-x}Ho_x$ FeO_3 thin films.

Samples	$a = b$ (Å)	c (Å)	V (Å^3)	D (Å)	t
BFO	5.5902	7.0520	190.84	245	0.912
$BHFO_{0.05}$	5.5966	6.9822	189.39	213	0.908
$BHFO_{0.10}$	5.6010	6.9592	189.06	184	0.905
$BHFO_{0.15}$	5.6093	6.8714	187.23	200	0.902
$BHFO_{0.20}$	5.6438	6.8207	188.01	147	0.898

Highlights

- Holmium-doped $BiFeO_3$ thin films have been investigated.
- Substitution of Bi with Ho modifies the lattice structure and the Fe^{2+} concentration.
- Doping with Holmium increases the saturation magnetization and decreases coercivity.
- The dielectric constant and loss tangent varies as a function of Holmium concentration.

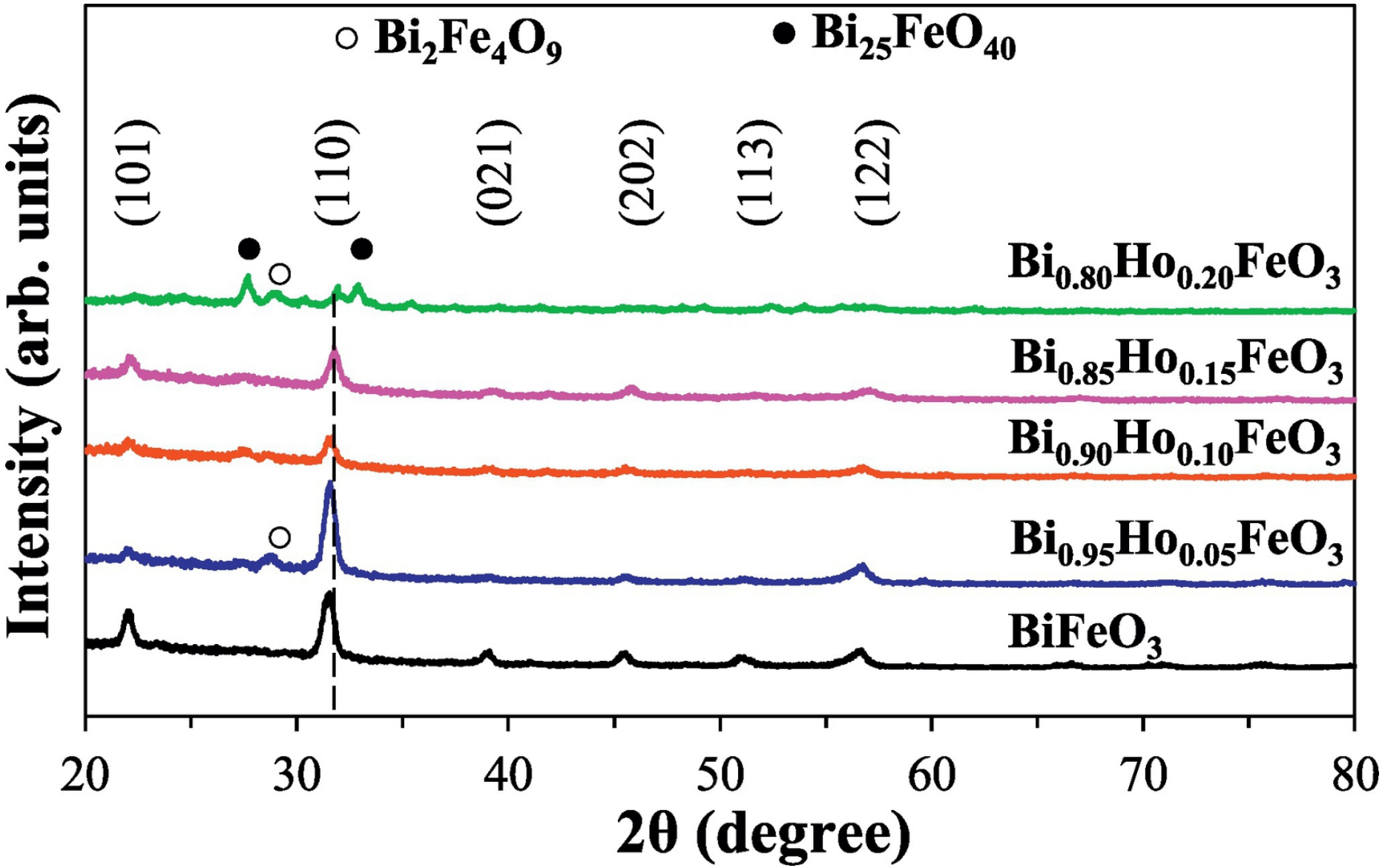
○ Bi2Fe4O9
● Bi25FeO40
(101)
(110)
(021)
(202)
(113)
(122)
Bi0.80Ho0.20FeO3
Bi0.85Ho0.15FeO3
Bi0.90Ho0.10FeO3
Bi0.95Ho0.05FeO3
BiFeO3
Intensity (arb. units)
20
30
40
50
60
70
80
2θ (degree)

Figure 1

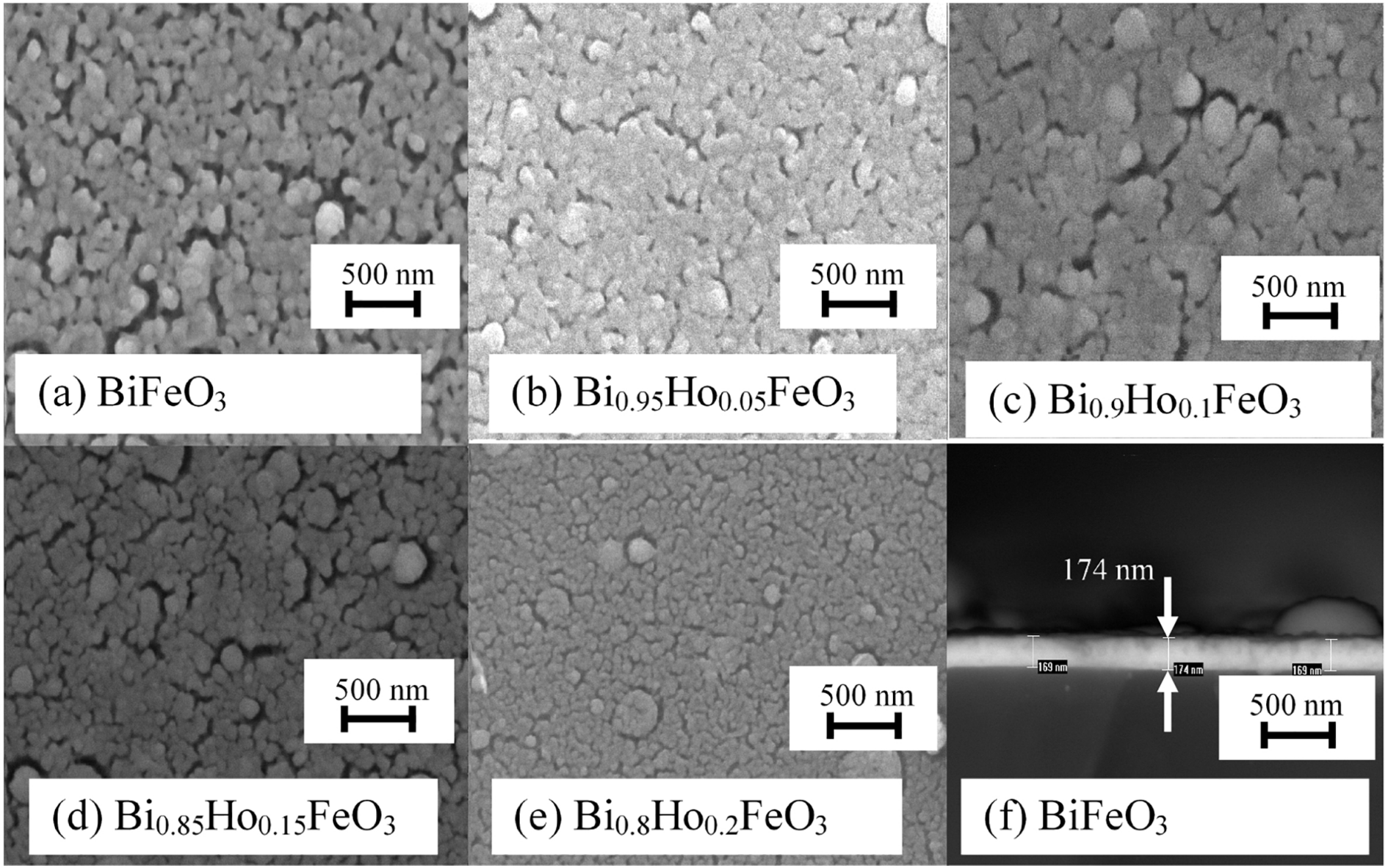
500 nm
(a) $BiFeO_3$
500 nm
(b) $Bi_{0.95}Ho_{0.05}FeO_3$
500 nm
(c) $Bi_{0.9}Ho_{0.1}FeO_3$
500 nm
(d) $Bi_{0.85}Ho_{0.15}FeO_3$
500 nm
(e) $Bi_{0.8}Ho_{0.2}FeO_3$
174 nm
169 nm
174 nm
169 nm
500 nm
(f) $BiFeO_3$

Figure 2

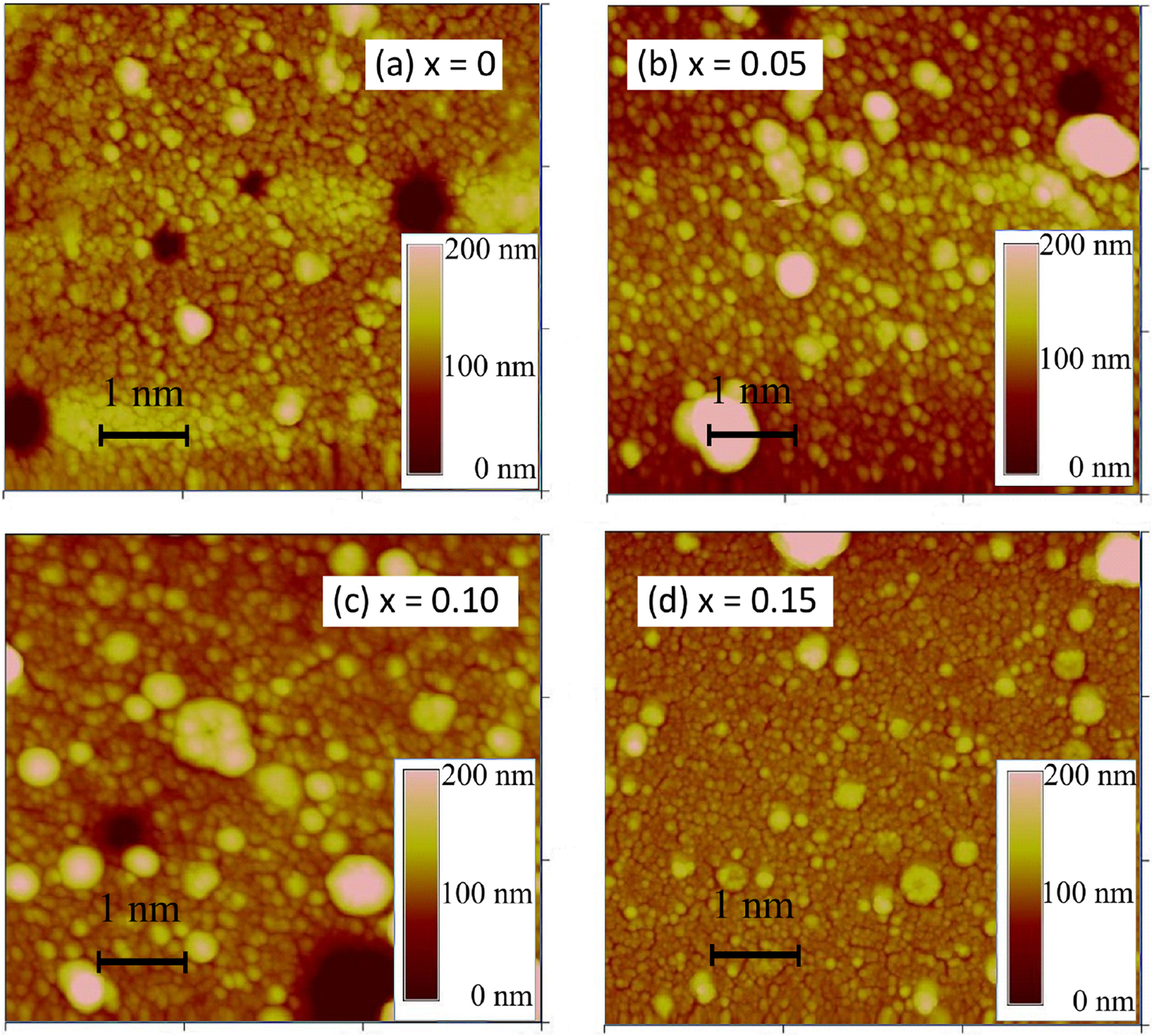
(a) x = 0
200 nm
100 nm
0 nm
1 nm
(b) x = 0.05
200 nm
100 nm
0 nm
1 nm
(c) x = 0.10
200 nm
100 nm
0 nm
1 nm
(d) x = 0.15
200 nm
100 nm
0 nm
1 nm

Figure 3

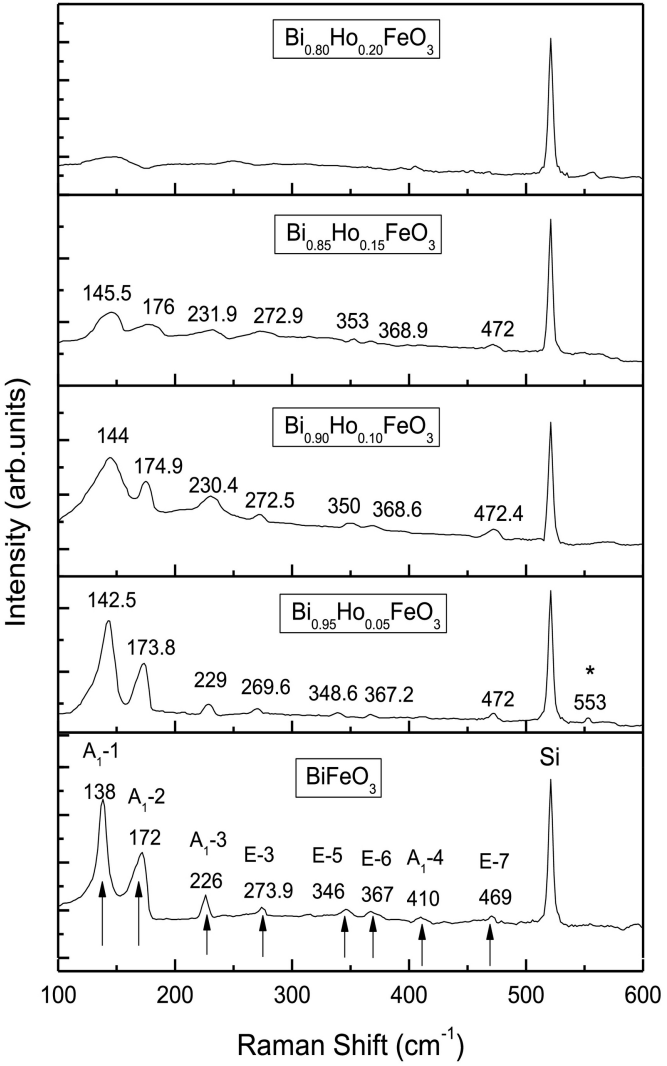
Bi0.80Ho0.20FeO3
Bi0.85Ho0.15FeO3
145.5
176
231.9
272.9
353
368.9
472
Bi0.90Ho0.10FeO3
144
174.9
230.4
272.5
350
368.6
472.4
Bi0.95Ho0.05FeO3
142.5
173.8
229
269.6
348.6
367.2
472
*
553
BiFeO3
A1-1
138
A1-2
172
A1-3
226
E-3
273.9
E-5
346
E-6
367
A1-4
410
E-7
469
Si
Intensity (arb.units)
100
200
300
400
500
600
Raman Shift (cm-1)

Figure 4

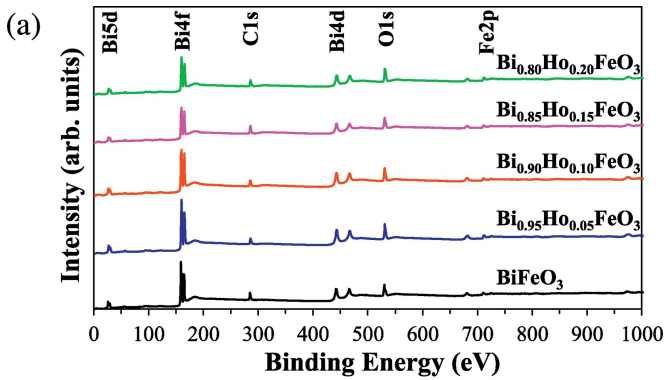
(a)
Bi5d
Bi4f
C1s
Bi4d
O1s
Fe2p
Bi0.80Ho0.20FeO3
Bi0.85Ho0.15FeO3
Bi0.90Ho0.10FeO3
Bi0.95Ho0.05FeO3
BiFeO3
Intensity (arb. units)
0 100 200 300 400 500 600 700 800 900 1000
Binding Energy (eV)

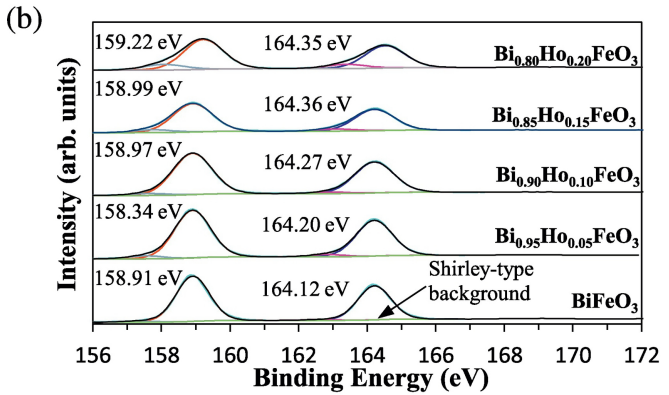
(b)
159.22 eV
164.35 eV
Bi0.80Ho0.20FeO3
158.99 eV
164.36 eV
Bi0.85Ho0.15FeO3
158.97 eV
164.27 eV
Bi0.90Ho0.10FeO3
158.34 eV
164.20 eV
Bi0.95Ho0.05FeO3
158.91 eV
164.12 eV
Shirley-type background
BiFeO3
Intensity (arb. units)
156 158 160 162 164 166 168 170 172
Binding Energy (eV)

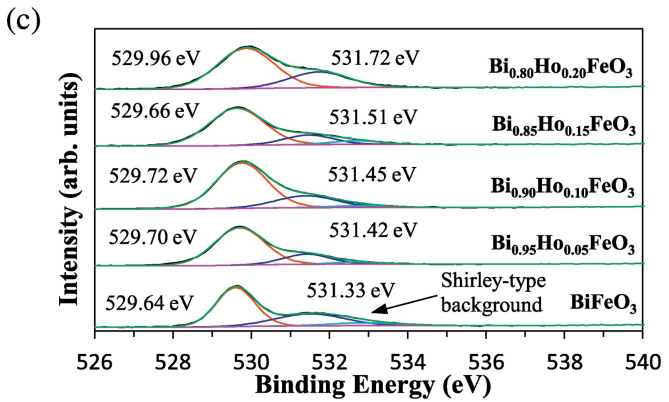
(c)
529.96 eV
531.72 eV
Bi0.80Ho0.20FeO3
529.66 eV
531.51 eV
Bi0.85Ho0.15FeO3
529.72 eV
531.45 eV
Bi0.90Ho0.10FeO3
529.70 eV
531.42 eV
Bi0.95Ho0.05FeO3
529.64 eV
531.33 eV
Shirley-type background
BiFeO3
Intensity (arb. units)
526 528 530 532 534 536 538 540
Binding Energy (eV)

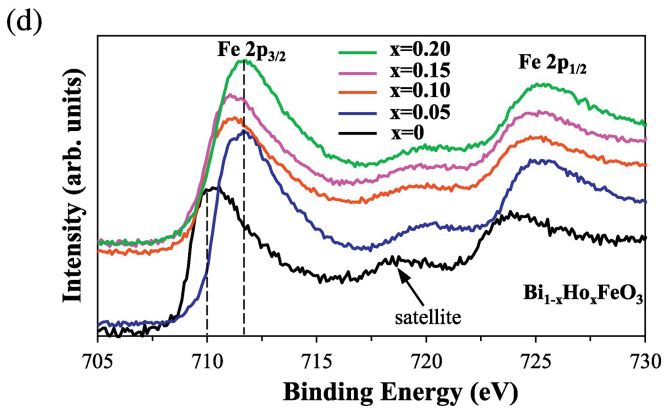
(d)
Fe 2p3/2
x=0.20
x=0.15
x=0.10
x=0.05
x=0
Fe 2p1/2
Bi1-xHoxFeO3
satellite
Intensity (arb. units)
705 710 715 720 725 730
Binding Energy (eV)

Figure 5

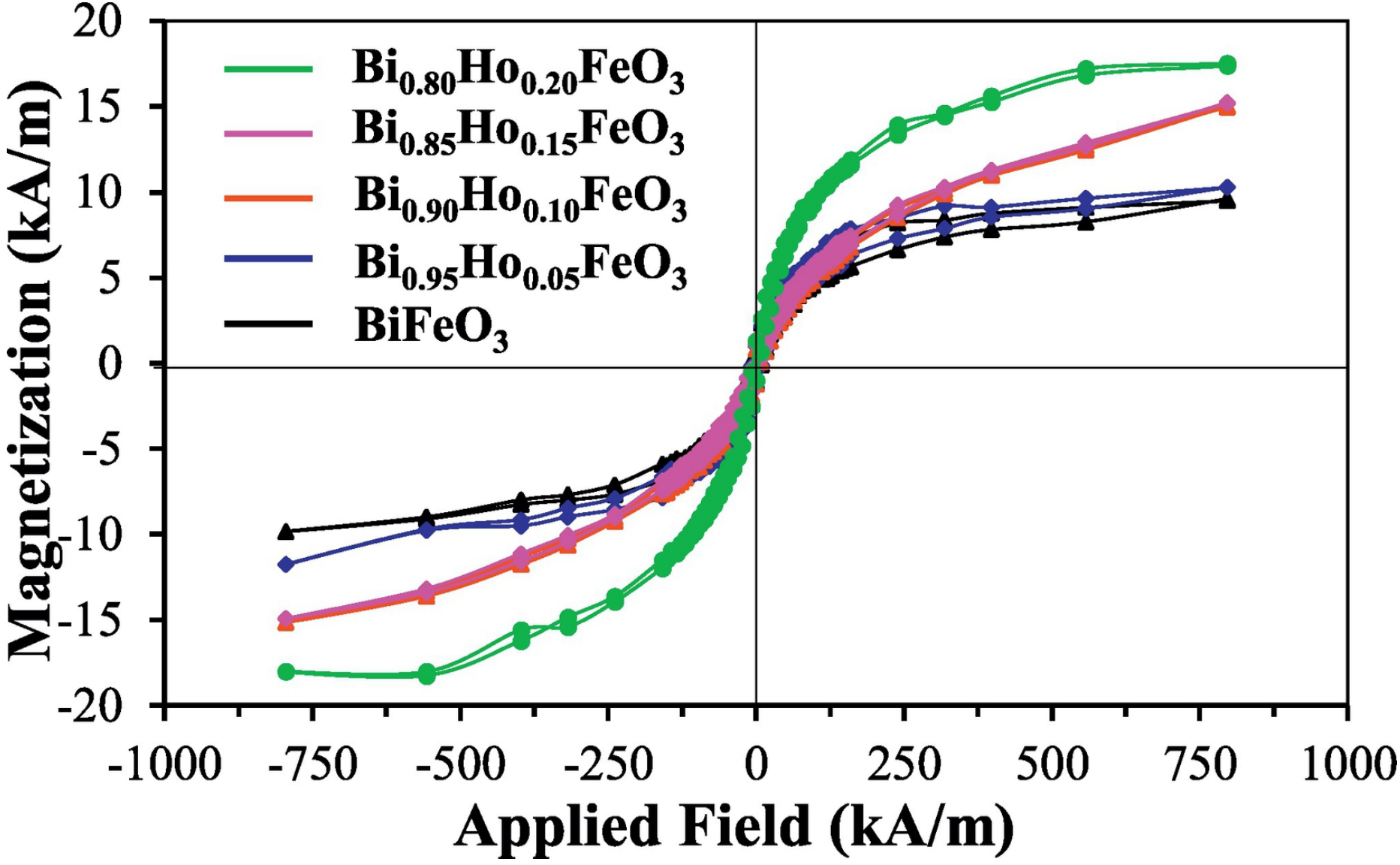
Bi0.80Ho0.20FeO3
Bi0.85Ho0.15FeO3
Bi0.90Ho0.10FeO3
Bi0.95Ho0.05FeO3
BiFeO3
Magnetization (kA/m)
Applied Field (kA/m)
20
15
10
5
0
-5
-10
-15
-20
-1000
-750
-500
-250
0
250
500
750
1000

Figure 6

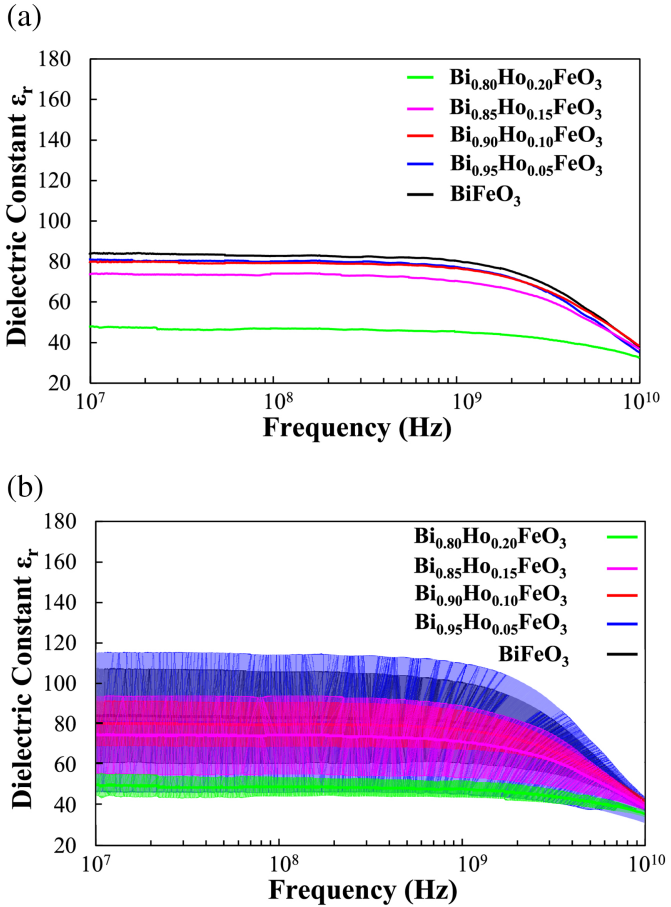
(a)
Dielectric Constant ε_r
Frequency (Hz)
$Bi_{0.80}Ho_{0.20}FeO_3$
$Bi_{0.85}Ho_{0.15}FeO_3$
$Bi_{0.90}Ho_{0.10}FeO_3$
$Bi_{0.95}Ho_{0.05}FeO_3$
$BiFeO_3$
(b)
Dielectric Constant ε_r
Frequency (Hz)
$Bi_{0.80}Ho_{0.20}FeO_3$
$Bi_{0.85}Ho_{0.15}FeO_3$
$Bi_{0.90}Ho_{0.10}FeO_3$
$Bi_{0.95}Ho_{0.05}FeO_3$
$BiFeO_3$

Figure 7

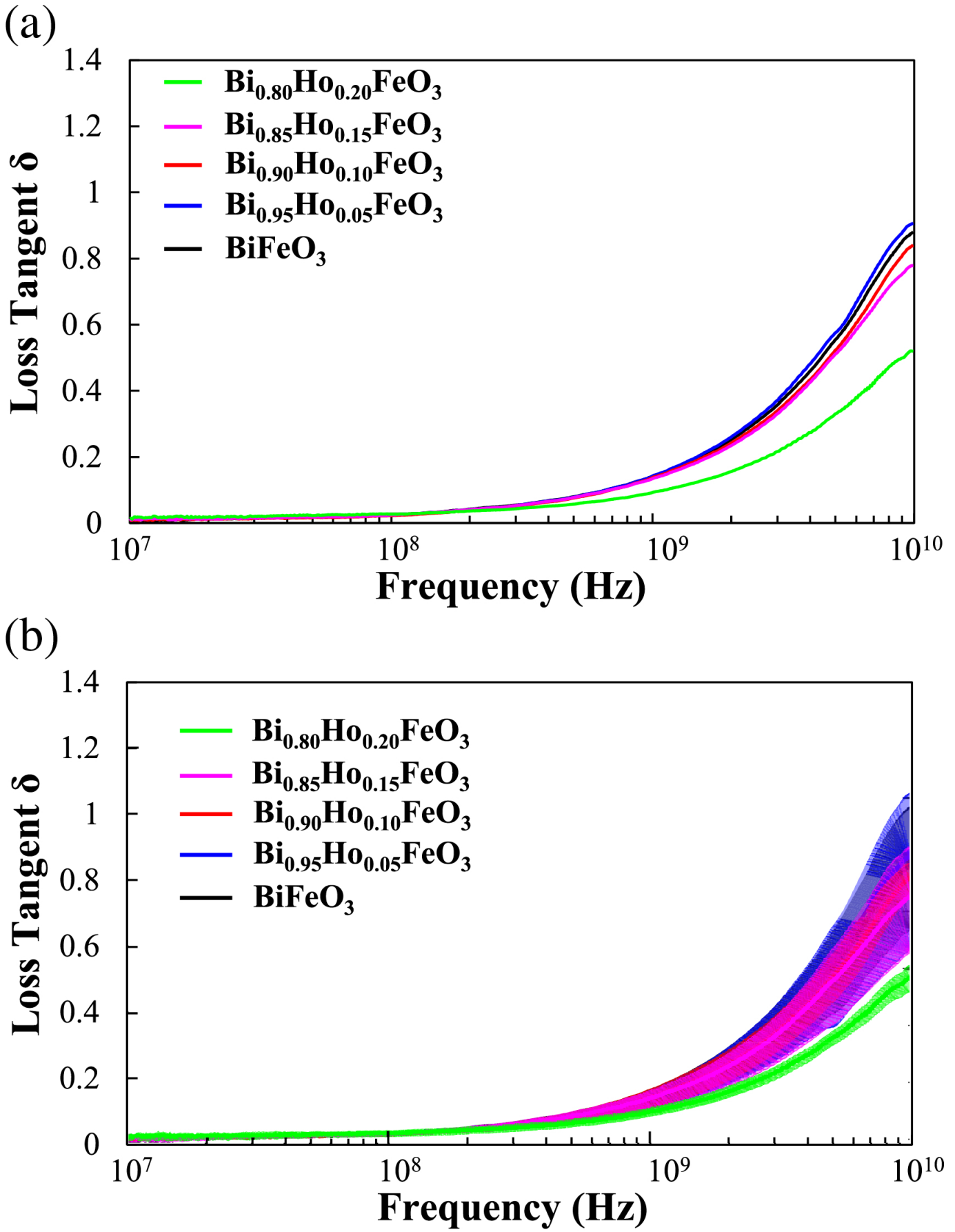
(a)
Loss Tangent δ
Frequency (Hz)
Bi0.80Ho0.20FeO3
Bi0.85Ho0.15FeO3
Bi0.90Ho0.10FeO3
Bi0.95Ho0.05FeO3
BiFeO3
(b)
Loss Tangent δ
Frequency (Hz)
Bi0.80Ho0.20FeO3
Bi0.85Ho0.15FeO3
Bi0.90Ho0.10FeO3
Bi0.95Ho0.05FeO3
BiFeO3

Figure 8